HJHPD

Article

Operational Silence and Climate-Driven Hidden Severe Malaria Burden in Sokoto State, Nigeria.

Received: 05.02.2026
Revised: 10.05.2026
Accepted: 12.05.2026
Published: 14.05.2026

Charles Adeiza Umar[1], Emmanuel Ndenor Sambo[2], Yakubu Joel Cherima[3]*, Zubairul Islam[4], Ajibili Megida[5], Maryamu Mbaya[6], Usman Mohammad Ibrahim[7], Yonwul Jacqueline Dakyen[8]

[1] Health Strategy and Leadership (HSL) Inc., Nigeria; cumar@hslhealth.pro; ORCID: https://orcid.org/0009-0001-1469-7983
[2] UKS Consulting Ltd, Nigeria; esambo@uksgroup.org; ORCID: https://orcid.org/0000-0002-5642-5433
[3] Center for AI Accountability in Health NG, Federal Capital Territory, Nigeria; ycherima@gmail.com; ORCID: https://orcid.org/0009-0004-3724-9886
[4] Faculty of Environmental Sciences, Hensard University, Bayelsa 56110, Nigeria; zubairul.islam@hensarduniversity.edu.ng; ORCID: https://orcid.org/0000-0002-6591-2241
[5] Pharmaceutical Society of Nigeria; bash2011meg@gmail.com; ORCID: https://orcid.org/0009-0001-0141-6118
[6] Department of Public Health, Babcock University, Ogun State, Nigeria; marymbaya090@gmail.com; ORCID: https://orcid.org/0009-0008-4918-9760
[7] Nigeria Centre for Disease Control and Prevention (NCDC), Nigeria; ibrahim.usman@ncdc.gov.ng; ORCID: https://orcid.org/0009-0009-9625-7671
[8] Independent Public Health Researcher, Nigeria; ydakyen@yahoo.com; ORCID: https://orcid.org/0009-0006-7229-4943

* Correspondence: ycherima@gmail.com

Abstract

Malaria remains a major public health challenge in northern Nigeria, where climatic suitability, weak healthcare accessibility, and operational surveillance limitations may contribute to the severe malaria burden. This study analyzed the temporal and spatial dynamics of severe malaria in Sokoto State, Nigeria, from 2014--2024 and estimated climate-driven hidden transmission zones via integrated geospatial modeling. The monthly severe malaria surveillance records for 23 LGAs were combined with climate variables, the Plasmodium falciparum parasite rate (PfPR), the population distribution, travel-time accessibility, and settlement indicators. Temporal trends were evaluated via Sen's slope and Mann–Kendall statistics, and a climate suitability index and accessibility-constrained hidden burden framework were developed to estimate the potential underdetected severe malaria burden. A total of 184,429 reported severe malaria cases were recorded from 2014–2024, with the highest annual burden observed in 2015 (22,404 cases). October presented the highest mean monthly burden (117.89 cases), whereas Sabon Birni recorded the highest cumulative severe malaria burden (28,943 cases). Climate-driven burden analysis identified Rabah (hidden burden ratio = 11.04), Kebbe (7.31), and Dange-Shuni (3.03) as major hidden burden hotspots characterized by high climate suitability and poor healthcare accessibility. Ward-level analysis further revealed highly localized operational silence zones within remote settlements. The findings demonstrate that integrating climate suitability with healthcare accessibility provides an effective framework for identifying hidden severe malaria transmission landscapes and operational surveillance gaps within semiarid environments.

Keywords: Malaria; Plasmodium falciparum parasite rate; climate suitability.

1. Introduction

Malaria remains one of the most significant public health challenges globally, particularly across sub-Saharan Africa, where environmental suitability, weak healthcare systems, and socioeconomic inequalities continue to sustain transmission dynamics [1,2]. Despite substantial improvements in malaria control during the past two decades, severe malaria continues to contribute considerably to morbidity and mortality in endemic regions, especially among vulnerable populations residing in environmentally favorable but poorly accessible areas [3,4]. Nigeria accounts for the largest proportion of the global malaria burden, contributing substantially to worldwide malaria cases and deaths annually [5]. Within Nigeria, northern states frequently experience persistent transmission because of favorable climatic conditions, population vulnerability, healthcare accessibility constraints, and operational limitations in surveillance systems [6,7].

Malaria transmission is strongly influenced by environmental and climatic conditions that regulate mosquito breeding, vector survival, parasite development, and human exposure patterns [8–10]. Temperature, rainfall, atmospheric moisture, soil moisture, and wind conditions are widely recognized as major environmental controls on malaria transmission dynamics [11,12]. In semiarid environments, relatively small variations in hydroclimatic conditions can substantially influence vector ecology and seasonal malaria transmission intensity [13]. Several studies have demonstrated that rainfall variability and temperature anomalies strongly affect malaria outbreaks and seasonal disease fluctuations across West Africa [14–16]. However, the magnitude and spatial expression of these relationships frequently vary according to local environmental conditions, settlement patterns, healthcare accessibility, and population density [17].

Recent advances in geospatial epidemiology have increasingly integrated remote sensing, spatial statistics, environmental suitability modeling, and healthcare accessibility analysis to improve the understanding of malaria transmission landscapes [18–20]. Spatial accessibility to healthcare facilities has emerged as a particularly important determinant of surveillance reliability and disease detection efficiency [21,22]. Populations residing in geographically isolated settlements commonly experience delayed diagnosis, reduced healthcare utilization, and lower reporting efficiency, thereby increasing the probability of hidden malaria burdens and operational surveillance gaps [23]. Consequently, reported surveillance records may substantially underestimate the true burden of severe malaria within remote and underserved regions.

The concept of operational silence has recently gained increasing relevance within public health surveillance research [24]. Operational silence refers to areas where limited healthcare accessibility, weak surveillance infrastructure, and reduced reporting efficiency create an apparent low disease burden despite persistent transmission risk [25]. Such conditions are particularly important in semiarid and rural African environments where dispersed settlements and weak healthcare accessibility constrain effective disease monitoring [26]. Nevertheless, most malaria studies in northern Nigeria continue to focus primarily on reported surveillance data without considering environmental suitability, accessibility limitations, or hidden burden estimation frameworks [27].

Sokoto State in northwestern Nigeria represents a particularly important environment for investigating climate-driven severe malaria dynamics and operational surveillance gaps. The state experiences high temperatures, strong rainfall seasonality, prolonged dry conditions, and substantial spatial heterogeneity in healthcare accessibility and settlement distribution. Therefore, rural and remote populations within Sokoto State may experience elevated hidden severe malaria burdens beyond officially reported surveillance records. Despite the epidemiological importance of the region, relatively few studies have integrated climate suitability, malaria endemicity, population exposure, and accessibility constraints to estimate hidden severe malaria transmission patterns across Sokoto State.

Several competing hypotheses exist regarding the dominant drivers of the malaria burden within semiarid African environments. Some studies argue that climatic suitability remains the primary determinant of transmission intensity [28,29], whereas others emphasize the dominant role of socioeconomic conditions, healthcare accessibility, and surveillance efficiency [30]. Additional studies suggest that malaria burden patterns emerge through complex interactions among environmental suitability, population exposure, settlement isolation, and healthcare infrastructure [31,32]. These contrasting perspectives highlight the need for integrated geospatial frameworks capable of simultaneously evaluating the environmental and operational determinants of severe malaria burden.

Therefore, the present study aimed to analyze the temporal and spatial dynamics of the severe malaria burden in Sokoto State between 2014 and 2024 and to estimate the climate-driven hidden severe malaria burden via environmental suitability, malaria endemicity, population distribution, and healthcare accessibility indicators. Specifically, this study sought to (1) evaluate temporal and spatial patterns of reported severe malaria burdens across LGAs in Sokoto State and (2) identify climate-driven hidden transmission hotspots and operational silence zones via integrated geospatial modeling approaches.

The results demonstrated substantial temporal and spatial heterogeneity in severe malaria burdens across Sokoto State, with strong seasonal concentrations during environmentally favorable transmission periods. The integrated climate-driven burden framework further identified multiple LGAs and wards characterized by elevated hidden transmission potential associated with high climate suitability, poor healthcare accessibility, and probable surveillance underreporting. These findings provide important insights for the strengthening of malaria surveillance, accessibility-focused intervention planning, and spatial prioritization of malaria control strategies within semiarid African environments.

2. Materials and methods

2.1 Study area

This study was conducted in Sokoto State, northwestern Nigeria, which is located approximately between latitudes 12°–14°N and longitudes 4°–7°E (Figure 1). Sokoto State shares an international boundary with the Republic of Niger and lies within the Sudan savannah ecological zone. The region experiences a semiarid tropical climate characterized by high temperatures, strong seasonal rainfall variability, prolonged dry conditions, and high evapotranspiration.

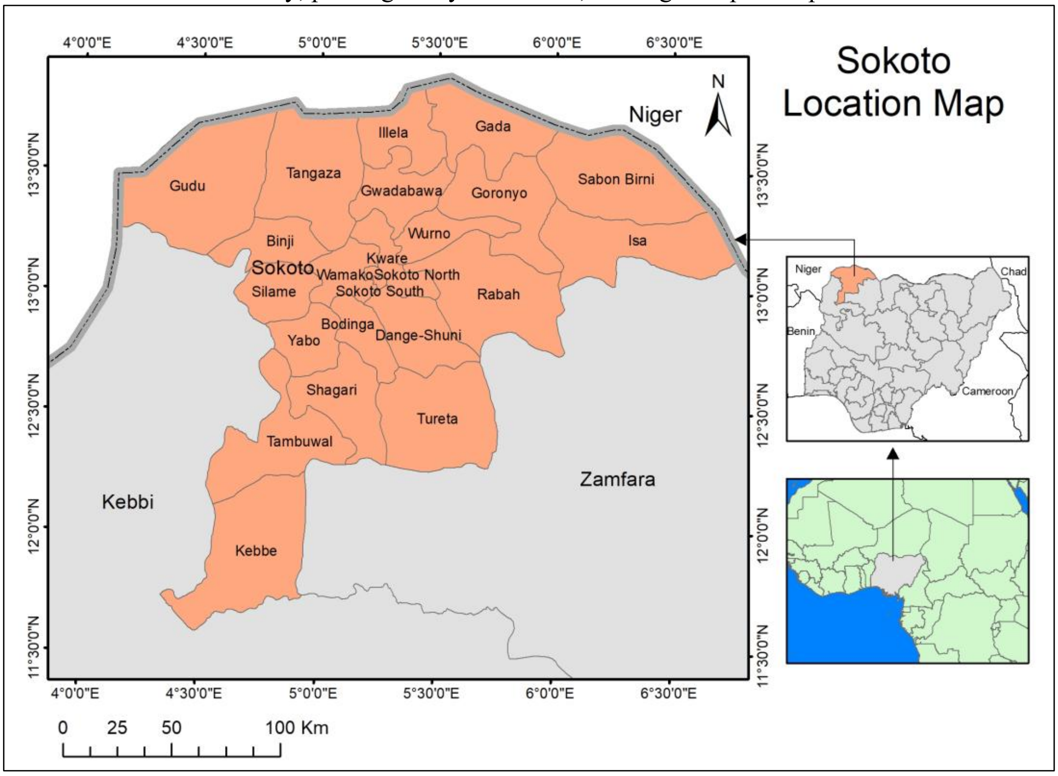

Figure 1. Location map of Sokoto State, northwestern Nigeria

Annual rainfall generally occurs between May and October, whereas the dry season extends from November to April under the influence of the Harmattan wind system. The mean annual temperatures commonly exceed 30°C, with extremely hot conditions during the prerainy season. These environmental conditions strongly influence mosquito ecology, malaria transmission dynamics, and the seasonal disease burden.

2.2 Study Design and Analytical Workflow

Figure 2 illustrates the overall study design and analytical workflow adopted for assessing the climate-driven hidden severe malaria burden and operational surveillance gaps across Sokoto State, Nigeria. The framework integrated severe malaria surveillance records (2014–2024), climate variables, malaria endemicity (PfPR), population exposure, healthcare accessibility, and health facility distribution within a standardized geospatial database. Temporal and spatial burden analyses were combined with climate suitability modeling to estimate the severe malaria burden. The HBI and HBN ratio (HBR) were subsequently derived to identify operational silence zones, accessibility-constrained transmission hotspots, and priority intervention areas for surveillance strengthening and malaria microplanning.

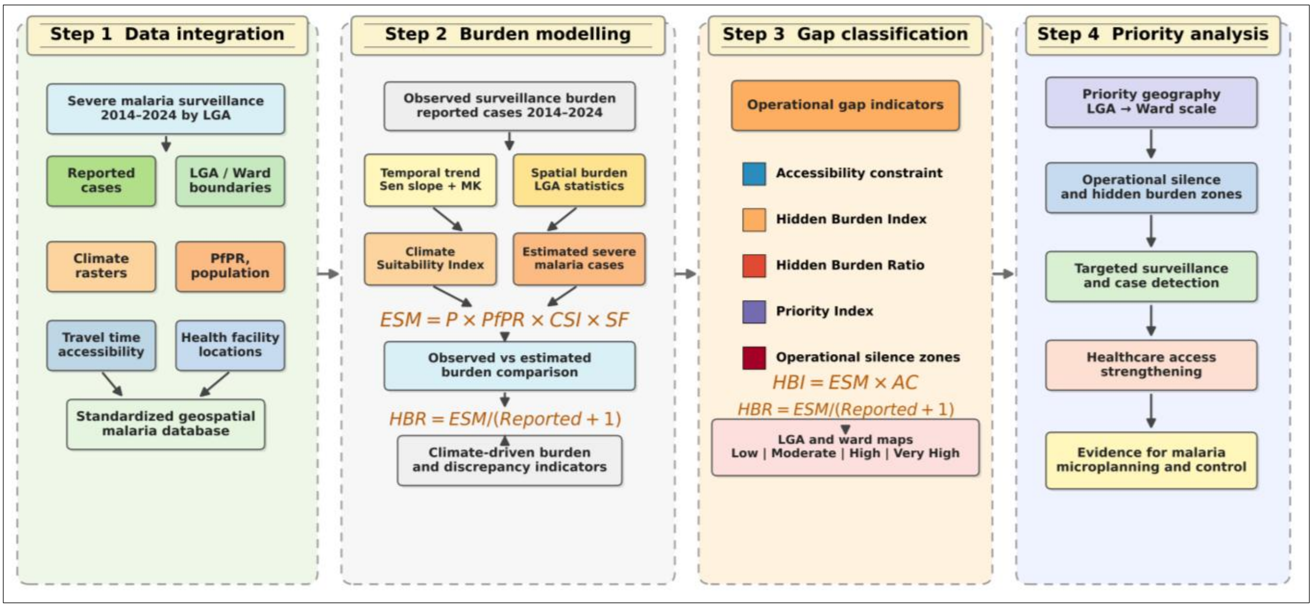

Figure 2. Conceptual study design and analytical workflow for assessing climate-driven hidden severe malaria burden and operational surveillance gaps in Sokoto State, Nigeria.

2.3 Data Sources

This study utilized multiple epidemiological, environmental, demographic, and accessibility datasets to assess the climate-driven severe malaria burden and operational surveillance gaps across Sokoto State, Nigeria (Table 1). Monthly severe malaria surveillance records (2014–2024) were obtained from the Nigerian DHIS2 platform. Administrative boundaries, health facility locations, population distributions, malaria endemicity (PfPR), climate variables, and healthcare accessibility datasets were integrated within a standardized geospatial framework. ERA5-Land climate variables were used to derive climate suitability conditions influencing malaria transmission, whereas travel-time accessibility analysis was employed to identify healthcare access limitations and probable operational silence zones across LGAs and underserved populations.

Table 1. Summary of epidemiological, environmental, demographic, and accessibility datasets used for assessing the climate-driven severe malaria burden and operational surveillance gaps in Sokoto State, Nigeria.

Dataset	Description	Source
Severe malaria surveillance data	Monthly severe malaria cases	https://dhis2nigeria.org.n [33]
Administrative Boundaries	State, LGA and Ward boundaries	https://data.humdata.org/ [34]
Health facilities	Health facility locations	https://data.grid3.org/ [35]
Population raster	Population distribution raster	https://www.worldpop.org/ [36]
Travel time raster	Travel time to healthcare facilities	Derived
Climate	Climate Variables	https://www.ecmwf.int/en/era5-land [37]
PfPR raster	Plasmodium falciparum parasite rate	https://malariaatlas.org/ [38, 39]

2.4 Severe Malaria Surveillance Processing

The monthly severe malaria surveillance records were transformed from wide tabular formats into long-format time series data to facilitate temporal statistical analysis. The data variables were reconstructed from monthly and yearly attributes. LGA names were standardized via uppercase conversion and whitespace normalization to ensure consistency during temporal aggregation and spatial integration.

Descriptive statistical indicators, including total cases, means, medians, standard deviations, and coefficients of variation, were computed at the monthly, annual, and LGA levels.

The coefficient of variation was estimated as:

$$CV = \frac{SD}{Mean} \tag{1}$$

where CV represents the coefficient of variation, SD represents the standard deviation, and $Mean$ represents the arithmetic mean of severe malaria cases.

Monthly climatological analysis was conducted to identify recurrent transmission peaks and temporal variability throughout the study period.

2.5 Trend analysis

Temporal trends in severe malaria burden were evaluated via Sen's slope estimator [40] and the Mann–Kendall trend test [41].

The Mann–Kendall statistic was computed as follows:

$$S = \sum_{i=1}^{n-1} \sum_{j=i+1}^{n} sgn(x_j - x_i) \tag{2}$$

where x_i and x_j represent observations at times i and j, respectively, and where n is the number of observations.

The sign function was defined as:

$$sgn(x_j - x_i) = \begin{cases} 1, & \text{if } (x_j - x_i) > 0 \\ 0, & \text{if } (x_j - x_i) = 0 \\ -1, & \text{if } (x_j - x_i) < 0 \end{cases} \tag{3}$$

Sen's slope estimator was calculated as follows:

$$Q_i = \frac{x_j - x_i}{j - i} \tag{4}$$

where Q_i represents the slope between observations x_i and x_j, and where i and j denote temporal positions.

The overall Sen's slope was estimated as the median of all pairwise slopes:

$$Q_{med} = Median(Q_i) \tag{5}$$

Kendall's tau coefficient was estimated as follows:

$$\tau = \frac{C - D}{0.5n(n-1)} \tag{6}$$

where C is the number of concordant pairs, D is the number of discordant pairs, and n is the total number of observations.

Positive tau values indicate increasing trends, whereas negative values indicate decreasing trends.

2.6 Climate suitability modeling

Climate suitability for malaria transmission was estimated via weighted integration of environmental variables associated with mosquito ecology and parasite development. The selected variables included rainfall, temperature, soil moisture, dew point moisture, solar radiation, and wind speed.

The wind speed was derived from the zonal and meridional wind components as follows:

$$Wind = \sqrt{U^2 + V^2} \tag{7}$$

where U represents the zonal wind component and where V represents the meridional wind component.

All the environmental variables were normalized between 0 and 1 via min–max normalization:

$$X_{norm} = \frac{X - X_{min}}{X_{max} - X_{min}} \tag{8}$$

where X_{norm} is the normalized variable, X is the original raster value, and X_{min} and X_{max} represent the minimum and maximum values, respectively.

The climate suitability index (CSI) was estimated as follows:

$$CSI = (0.30R) + (0.25T) + (0.20S) + (0.15D) + (0.05W) + (0.05SR) \tag{9}$$

where CSI is the climate suitability index; R, T, S, D, W, and SR represent the rainfall, temperature, soil moisture, dew point, wind, and solar radiation suitability scores, respectively.

Higher weights were assigned to rainfall and temperature because of their dominant influence on mosquito breeding conditions and malaria transmission dynamics within semiarid environments.

2.7 Estimation of Climate-Driven Severe Malaria Burden

The climate-driven severe malaria burden was estimated by integrating population exposure, malaria endemicity, climate suitability, and the severe disease fraction.

The estimation model was expressed as follows:

$$ESM = P \times PfPR \times CSI \times SF \tag{10}$$

where ESM is the estimated severe malaria burden, P is the exposed population, $PfPR$ is the *Plasmodium falciparum* parasite rate, CSI is the climate suitability index, and SF is the severe malaria fraction used to estimate the proportion of malaria infections progressing to severe disease.

A severe malaria fraction of 0.005 was used to approximate the proportion of malaria infections progressing to severe disease.

2.8 Accessibility and Hidden Burden Modeling

Healthcare accessibility constraints were estimated via travel-time rasters, which represent movement difficulty and healthcare accessibility limitations.

The accessibility constraint was normalized as:

$$AC = \frac{TT - TT_{min}}{TT_{max} - TT_{min}} \tag{11}$$

where AC is the accessibility constraint and where TT is the travel time to the nearest healthcare facility, with higher AC values indicating greater healthcare accessibility limitations and an increased likelihood of surveillance gaps.

The HBI was estimated as follows:

$$HBI = ESM \times AC \tag{12}$$

where HBI is the HBI, ESM is the estimated severe malaria burden, and AC is the accessibility constraint, such that higher HBI values indicate greater potential hidden severe malaria burdens associated with limited healthcare accessibility.

The HBN ratio (HBR) was computed as follows:

$$HBR = \frac{Estimated\ Severe\ Cases}{Reported\ Severe\ Cases + 1} \tag{13}$$

where the constant 1 prevents division-by-zero errors.

Higher HBR values indicate probable underreporting and operational surveillance gaps associated with poor healthcare accessibility.

A priority index (PI) was additionally estimated to identify hidden transmission hotspots via normalized climate suitability, malaria prevalence, population exposure, and accessibility indicators:

$$PI = CSI_{norm} \times PfPR_{norm} \times P_{norm} \times AC_{norm} \tag{14}$$

where PI is the priority index, CSI_{norm} is the normalized climate suitability index, $PfPR_{norm}$ is the normalized *Plasmodium falciparum* parasite rate, P_{norm} is the normalized population exposure, and AC_{norm} is the normalized accessibility constraint. Higher PI values indicate areas requiring greater priority for malaria surveillance, intervention, and healthcare access improvement.

2.9 Statistical analysis

Temporal and spatial variations in severe malaria burden were evaluated via analysis of variance (ANOVA), Kruskal–Wallis nonparametric tests, linear regression, Sen's slope estimation, Mann–Kendall trend analysis, and Kendall correlation statistics. ANOVA was used to assess differences among groups where assumptions of normality were satisfied, whereas the Kruskal–Wallis test was applied to nonnormally distributed malaria case data. Linear regression was used to quantify long-term trends, whereas Sen's slope and Mann–Kendall statistics were employed to estimate trend magnitude and significance, respectively. Kendall correlation analysis was used to evaluate associations among epidemiological and environmental variables. Statistical significance was assessed at the 95% confidence level ($p < 0.05$).

2.10 Spatial analysis and mapping

Spatial integration and zonal aggregation were performed at both the LGA and ward levels to support multiscale assessment of severe malaria burden and surveillance performance. Choropleth maps, burden ranking maps, heatmaps, and spatial trend visualizations were generated to examine the geographic distributions of severe malaria burdens, temporal malaria trends, climate-driven hidden transmission hotspots, healthcare accessibility constraints, and operational silence zones. These spatial analyses facilitated the identification of high-risk areas, probable surveillance gaps, and priority locations for targeted malaria intervention and healthcare accessibility improvement.

2.11 Software environment and reproducibility

All analyses were conducted via the R statistical environment (R version 4.5.x). The major libraries included sf, terra, dplyr, tidyr, ggplot2, Kendall, viridis, readr, stringr, and lubridate.

All preprocessing, statistical analyses, spatial aggregation, and cartographic procedures were implemented through scripted workflows to ensure analytical reproducibility, transparency, and minimal manual intervention. Spatial processing and mapping were conducted via open-source geospatial analytical workflows.

3. Results

3.1 Temporal and Spatial Patterns of Severe Malaria Burden in Sokoto State (2014–2024)

A total of 184,429 reported severe malaria cases were recorded across Sokoto State between 2014 and 2024, demonstrating substantial temporal and spatial variability in disease burden (Figure 3). Annual severe malaria cases were highest in 2015 (22,404 cases), followed by 2014 (19,406 cases), while relatively lower burdens were observed after 2018, particularly from 2021–2024. Pronounced spatial heterogeneity was additionally observed among the LGAs. Sabon Birni recorded the highest cumulative burden (28,943 cases), followed by Gada (22,772 cases) and Illela (13,759 cases), whereas Gudu presented the lowest burden (1,177 cases) (Figure 4).

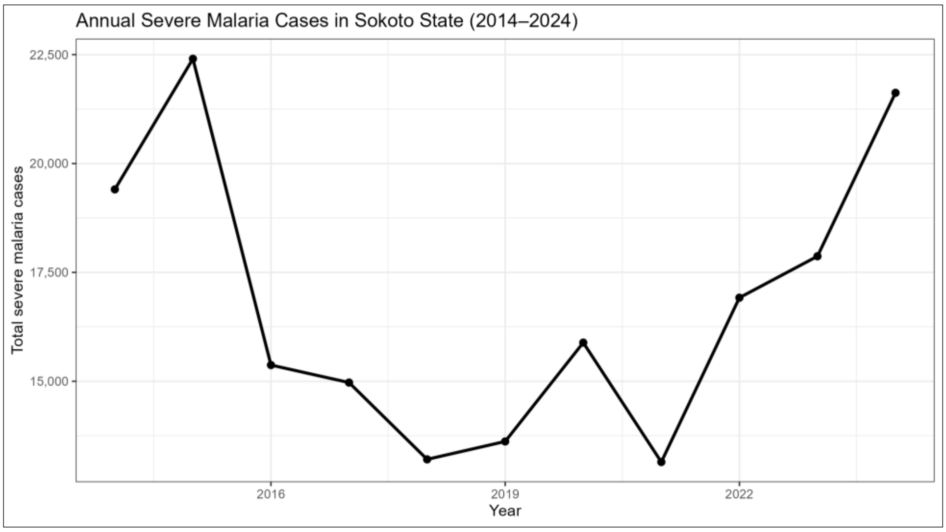

Figure 3. Annual trend of reported severe malaria cases in Sokoto State, Nigeria, from 2014--2024.

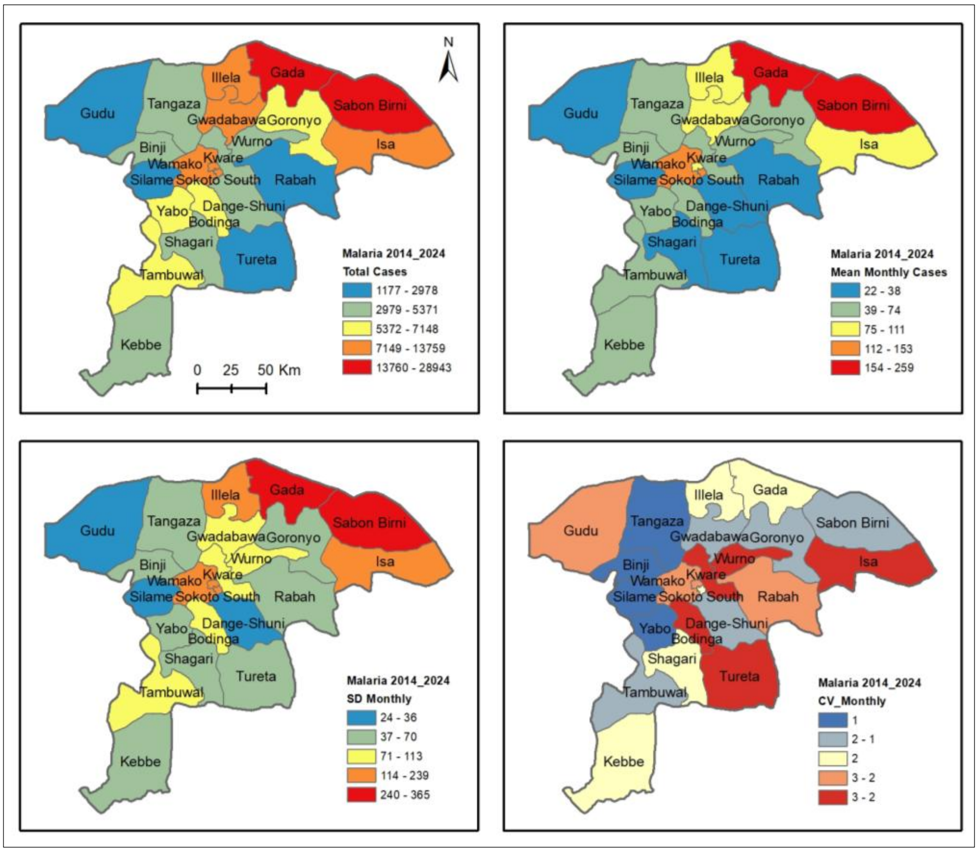

Figure 4. Spatial distributions of the cumulative severe malaria burden (2014–2024), mean monthly cases, monthly variability (standard deviation), and coefficient of variation across LGAs in Sokoto State, Nigeria.

The mean number of monthly severe malaria cases ranged from 21.80 in Gudu to 258.77 in Gada. Several LGAs, including Tureta (CV = 2.26), Kware (2.05), and Isa (1.93), demonstrated high temporal variability, indicating unstable transmission dynamics and strong intermonthly fluctuations in severe malaria occurrence (Figure 5).

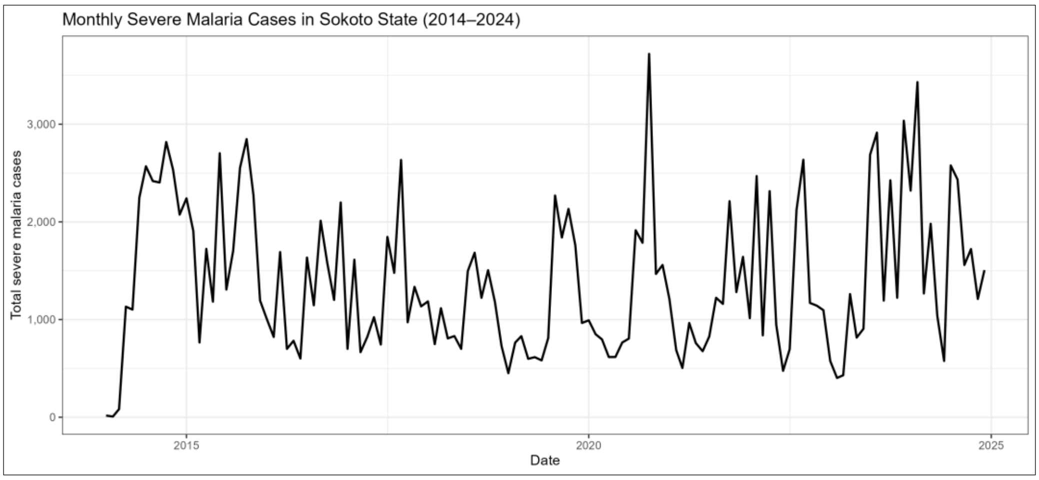

Figure 5. Monthly temporal dynamics of reported severe malaria cases in Sokoto State, Nigeria, from January 2014 to December 2024, showing substantial intermonthly variability and recurrent transmission peaks across the study period.

Monthly climatological analysis revealed pronounced seasonal malaria dynamics throughout the study period. In October, the highest mean monthly burden (117.89 cases) was recorded, whereas in March, the lowest mean burden (53.49 cases) was recorded. The seasonal ratio between the peak and lowest transmission months was 2.20, indicating strong seasonality in severe malaria occurrence across Sokoto State (Figure 6).

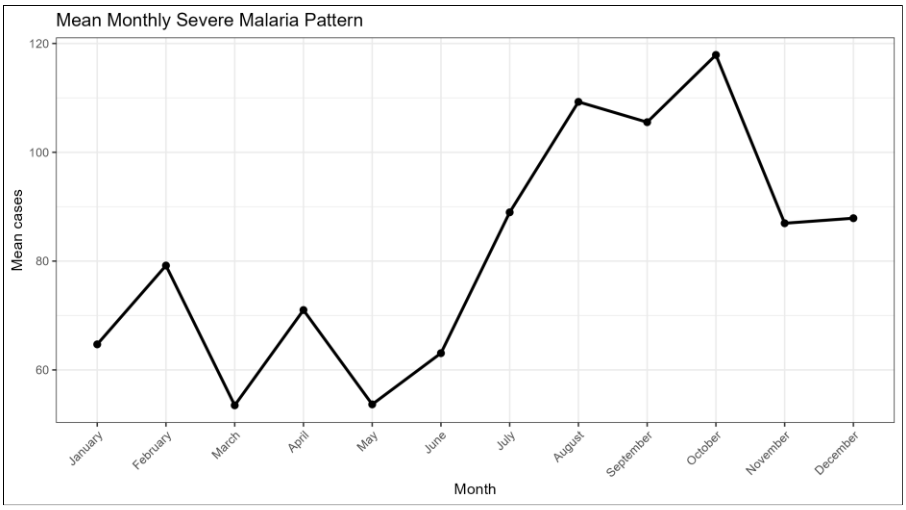

Figure 6. Monthly temporal variability of reported severe malaria cases in Sokoto State, Nigeria, from January 2014 to December 2024.

Seasonal aggregation further revealed clear transmission concentrations during the rainy period. The peak rainy season contributed the largest proportion of severe malaria burden cases, accounting for 59,567 cases (32.30% of total reported cases), followed by the dry season, with 51,534 cases (27.94%). The postpeak and prepeak rainy seasons contributed 21.53% and 18.23% of the total cases, respectively. These findings indicate strong hydroclimatic control on malaria transmission dynamics within the semiarid environment of Sokoto State.

Substantial spatial heterogeneity in severe malaria burden was observed among LGAs. Sabon Birni reported the highest cumulative severe malaria burden from 2014–2024, with 28,943 reported cases, followed by Gada

(22,772 cases), Illela (13,759 cases), Gwadabawa (10,865 cases), and Sokoto South (10,845 cases). Several LGAs additionally exhibited high coefficients of variation, indicating unstable temporal transmission patterns and substantial monthly variability.

Trend analysis revealed mixed spatial trends in severe malaria burdens across the state. Positive Sen's slope values indicated increasing severe malaria burdens in several LGAs, particularly Bodinga (Sen's slope = 94.38 cases year^{-1}), Gada (107.00 cases year^{-1}), and Binji (32.50 cases year^{-1}). In contrast, Dange-Shuni exhibited a strong decreasing trend (Sen's slope = −50.89 cases year^{-1}). However, state-level Mann–Kendall analysis indicated an overall weak long-term increasing tendency ($\tau = 0.018$) that was statistically nonsignificant ($p = 1.00$) (Figure 7).

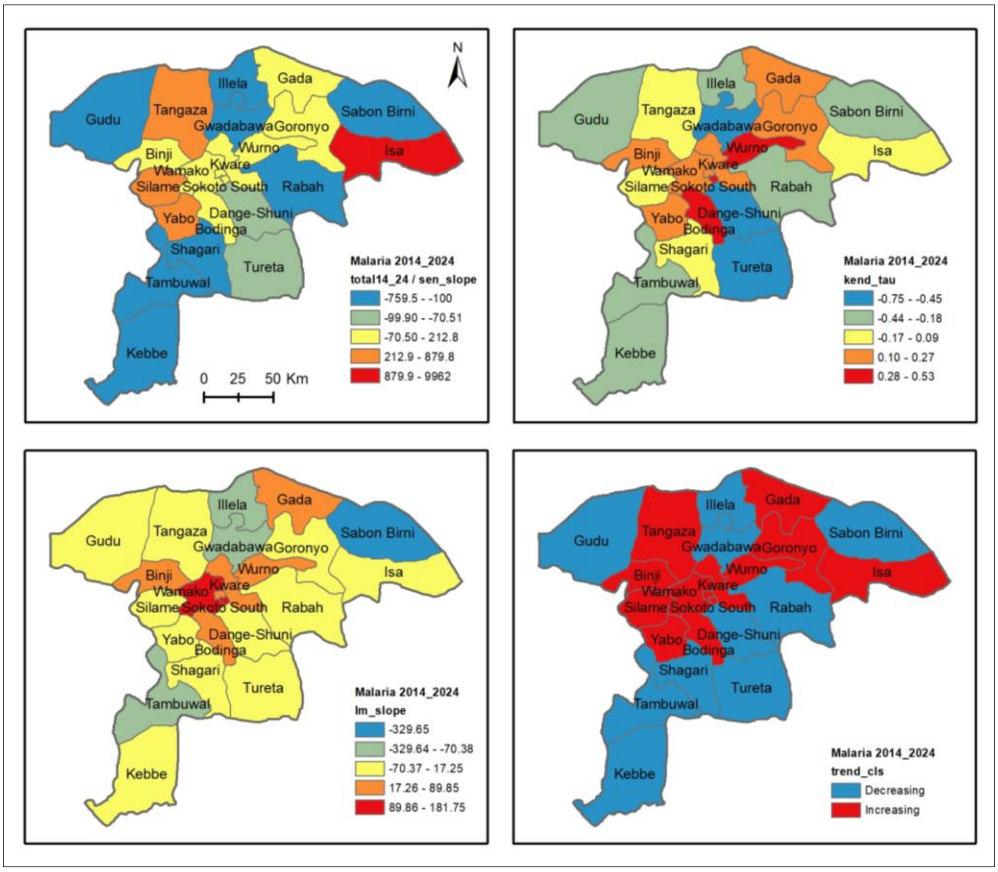

Figure 7. Spatial patterns of severe malaria temporal dynamics across Sokoto State, Nigeria, including total cases, Sen's slope trend magnitude, linear trend slope, and increasing/decreasing malaria trend direction for the period of 2014–2024.

Statistical hypothesis testing confirmed significant temporal, seasonal, and spatial variability in severe malaria burden across Sokoto State. Kruskal–Wallis analysis revealed significant interannual variation among years ($\chi^2 = 48.64$, $df = 10$, $p < 0.001$), significant seasonal variation ($\chi^2 = 61.66$, $df = 3$, $p < 0.001$), and highly significant spatial variation among LGAs ($\chi^2 = 447.56$, $df = 22$, $p < 0.001$). These findings indicate that the severe malaria burden in Sokoto State is strongly influenced by spatial heterogeneity and seasonal environmental conditions.

3.2 Climate-Driven Severe Malaria Burden and Hidden Transmission Zones

3.2.1 Spatial Patterns of Climate Suitability, Accessibility Constraint, and Estimated Severe Malaria Burden

Figure 8 shows the spatial distributions of climate suitability, malaria endemicity, population exposure, accessibility constraints, and estimated climate-driven severe malaria burdens across Sokoto State. Considerable spatial heterogeneity was observed among the LGAs for all the modeled variables.

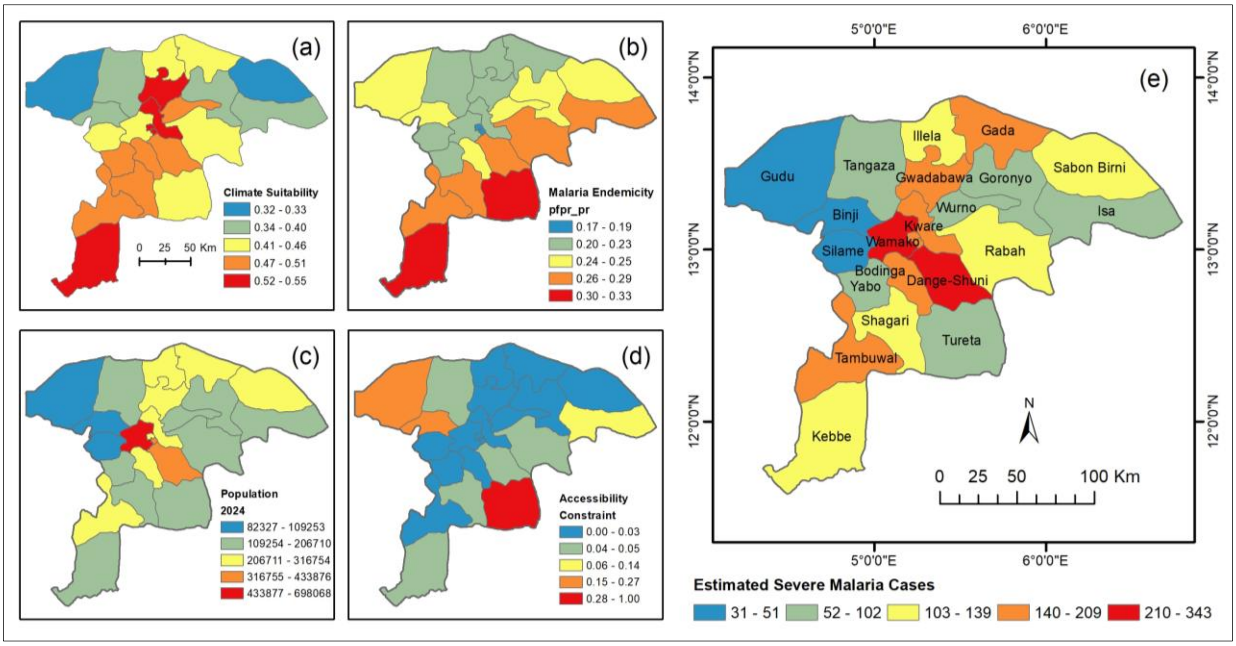

Figure 8. Spatial distributions of climate suitability, malaria endemicity (PfPR), population exposure, healthcare accessibility constraints, and estimated climate-driven severe malaria burdens across LGAs in Sokoto State, Nigeria.

The climate suitability values ranged from 0.32 to 0.55, indicating generally favorable environmental conditions for malaria transmission throughout Sokoto State (Figure 9a). The highest climate suitability values were observed in Gwadabawa (0.55), Kware (0.54), Sokoto North (0.54), Sokoto South (0.54), and Kebbe (0.53), whereas Gudu (0.32) and Sabon Birni (0.33) presented comparatively lower suitability values. These findings indicate that central and southern LGAs generally experience more favorable environmental conditions for sustained malaria transmission.

Malaria endemicity (PfPR) additionally demonstrated substantial spatial variability (Figure 9b). The PfPR values ranged from 0.17 in Sokoto South to 0.33 in Kebbe. Elevated endemicity was particularly observed in Kebbe (0.33), Tureta (0.31), Rabah (0.29), Isa (0.28), and Tambuwal (0.28), suggesting relatively high malaria transmission intensities within these LGAs.

The population exposure varied considerably across the state (Figure 9c). Wamako presented the highest exposed population (698,068 persons), followed by Sokoto South (433,876 persons) and Dange-Shuni (385,627 persons). In contrast, Gudu presented the lowest exposed population (82,327 persons). The concentration of large populations within environmentally suitable LGAs substantially increased the estimated severe malaria burden.

Accessibility constraint analysis revealed marked spatial inequality in healthcare accessibility across Sokoto State (Figure 9d). The accessibility constraint values ranged from 0.00--1.00. Tureta presented the highest accessibility constraint (1.00), followed by Gudu (0.24) and Isa (0.14), indicating substantial healthcare accessibility limitations and an increased probability of surveillance gaps within these LGAs. In contrast, Sokoto South (0.00) and Sokoto North (0.002) presented relatively favorable healthcare accessibility conditions.

The integrated climate-driven severe malaria burden model demonstrated strong spatial clustering of estimated severe malaria cases across the state (Figure 9e). The estimated severe malaria burden ranged from approximately 31--343 cases among LGAs. Wamako recorded the highest estimated severe malaria burden (342.92 cases), followed by Dange-Shuni (257.47 cases), Tambuwal (209.14 cases), Sokoto South (200.97 cases), and Bodinga (194.24 cases). In contrast, Gudu presented the lowest estimated burden (31.34 cases). Several LGAs characterized by elevated climate suitability, increased malaria endemicity, large exposed populations, and accessibility constraints presented disproportionately high estimated severe malaria burdens, indicating probable hidden transmission potential and operational surveillance limitations.

Overall, the integrated spatial framework demonstrated that climate suitability, malaria endemicity, population exposure, and healthcare accessibility collectively govern the spatial distribution of severe malaria burdens across Sokoto State.

3.2.2 Accessibility Constraint and Hidden Burden Index

Figure 9 illustrates the spatial distribution of healthcare accessibility constraints and the HBI across Sokoto State. Considerable spatial heterogeneity was observed in both accessibility limitations and severe malaria burdens among LGAs.

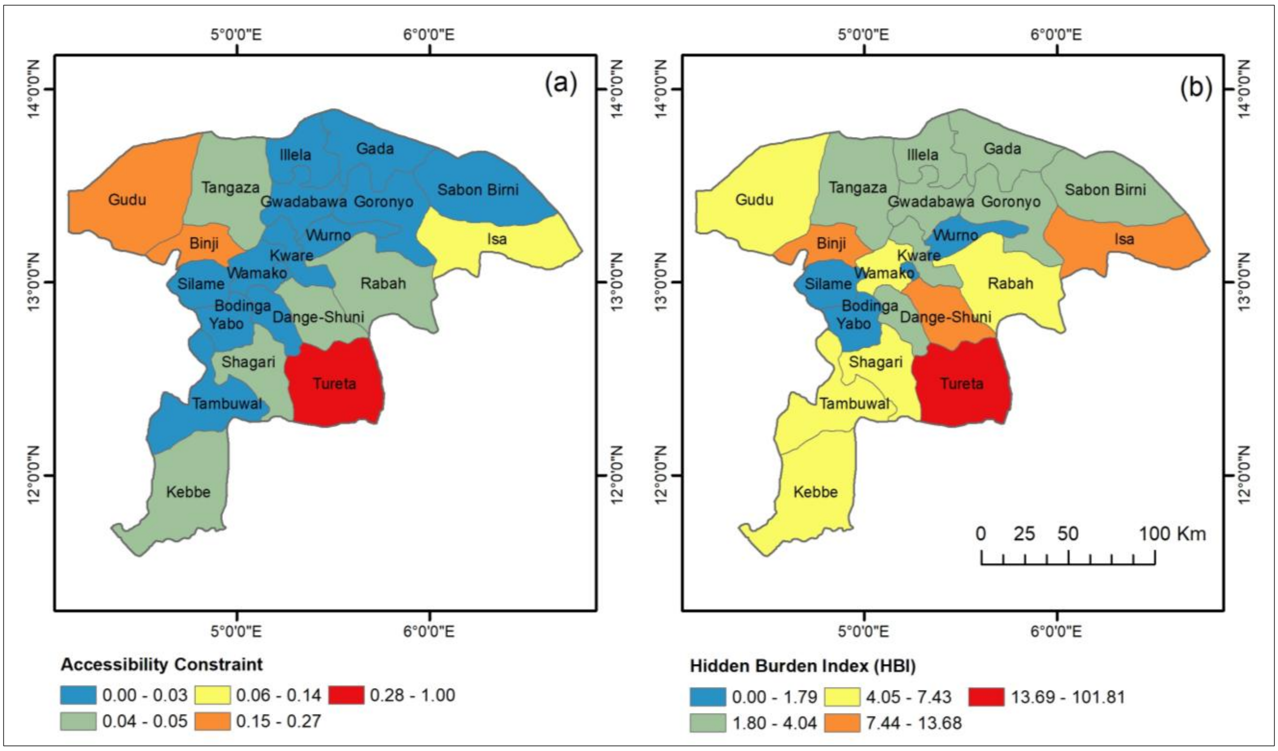

Figure 9. Spatial distribution of healthcare accessibility constraints and the HBI across LGAs in Sokoto State, Nigeria, highlighting operational surveillance gaps and probable hidden severe malaria transmission zones.

The accessibility constraint values ranged from 0.00--1.00 (Figure 10a). Tureta presented the highest accessibility constraint (1.00), indicating extremely poor healthcare accessibility and substantial operational limitations in accessing diagnosis and treatment services. Elevated accessibility constraints were additionally observed in Binji (0.27), Gudu (0.24), and Isa (0.14), whereas Sokoto South (0.00) and Sokoto North (0.002) demonstrated relatively favorable healthcare accessibility conditions. Most central and urbanized LGAs presented comparatively lower accessibility constraints (<0.05), suggesting relatively improved healthcare connectivity and reduced travel difficulty.

The HBI demonstrated pronounced spatial concentration within accessibility-constrained LGAs (Figure 10b). The HBI values ranged from 0.00 to 101.81, indicating substantial variability in the probable hidden severe malaria burden across the state. Tureta recorded the highest HBI value (101.81), substantially exceeding all the other LGAs, followed by Binji (13.68), Isa (11.16), and Dange-Shuni (10.29). Elevated HBI values were also observed in Gudu (7.43), Shagari (6.01), Kebbe (5.93), Tambuwal (5.66), and Rabah (5.64).

In contrast, Sokoto South presented an HBI value of 0.00, whereas Sokoto North (0.37), Silame (0.88), and Yabo (1.65) presented comparatively low hidden burden conditions. The lower HBI values within these LGAs correspond closely with improved healthcare accessibility and reduced accessibility constraints.

The strong spatial association between accessibility limitations and elevated HBI values indicates that poor healthcare accessibility substantially contributes to the probable underdetection of severe malaria burdens within several LGAs. In particular, remote and underserved LGAs characterized by increased travel difficulty presented disproportionately high hidden burden conditions despite moderate or relatively lower reported surveillance records.

3.2.3 Hidden Burden Ratio and Operational Surveillance Gaps

Figure 10 shows the spatial distribution of the cumulative reported severe malaria burden (2014–2024), estimated climate-driven severe malaria burden, and Hidden Burden Ratio (HBR) across Sokoto State. Considerable discrepancies were observed between reported surveillance records and estimated severe malaria burdens among several LGAs, indicating probable operational surveillance gaps and hidden transmission potential.

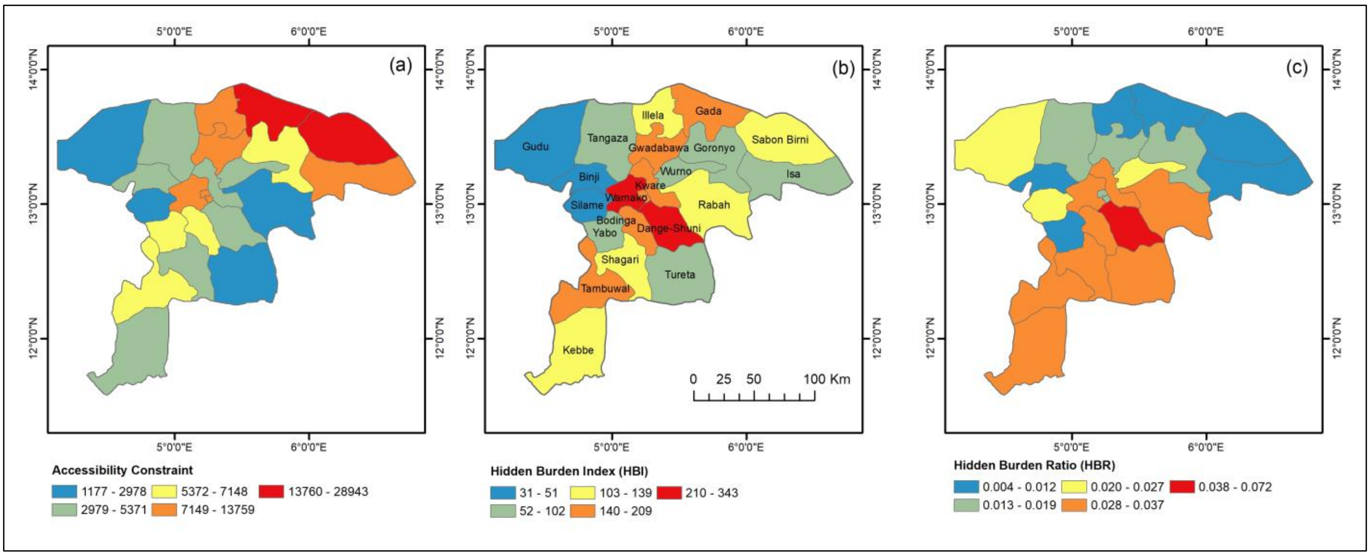

Figure 10. Spatial distribution of the cumulative reported severe malaria burden (2014–2024), estimated climate-driven severe malaria burden, and Hidden Burden Ratio (HBR) across LGAs in Sokoto State, Nigeria, highlighting probable operational surveillance gaps and hidden transmission zones.

The reported severe malaria burden demonstrated substantial spatial variability across the state (Figure 11a). Sabon Birni recorded the highest cumulative reported burden (28,943 cases), followed by Gada (22,772 cases) and Illela (13,759 cases), whereas Gudu presented the lowest cumulative burden (1,177 cases). Several northern and eastern LGAs demonstrated relatively high reported severe malaria burdens compared with the central and western sectors of the state.

The estimated climate-driven severe malaria burden additionally exhibited pronounced spatial clustering (Figure 11b). Goronyo recorded the highest estimated severe malaria burden (342.92 cases), followed by Binji (257.47 cases), Illela (209.14 cases), Bodinga (194.24 cases), and Shagari (179.62 cases). An elevated estimated burden was generally associated with favorable climatic suitability, substantial population exposure, and moderate accessibility constraints.

The Hidden Burden Ratio (HBR) revealed substantial spatial variation in the discrepancy between the estimated and reported severe malaria burdens (Figure 11c). The HBR values ranged from 0.0039 to 0.0717 across Sokoto State. Binji presented the highest HBR value (0.0717), followed by Bodinga (0.0371), Dange-Shuni (0.0358), Gada (0.0350), and Goronyo (0.0347). In contrast, Yabo (0.0039), Wurno (0.0069), and Wamako (0.0079) demonstrated comparatively lower HBR values, indicating relatively stronger agreement between the estimated and reported burdens.

LGAs characterized by elevated HBR values generally present moderate-to-high estimated climate-driven burdens with comparatively lower reported surveillance burdens, suggesting probable underreporting and operational surveillance limitations. Several LGAs with high HBR values additionally presented moderate-to-high accessibility constraints and environmental suitability, further indicating the influence of healthcare accessibility limitations on surveillance efficiency.

The spatial coincidence of elevated HBR values with accessibility-constrained and environmentally favorable LGAs strongly suggests that routine surveillance systems may underestimate the true severe malaria burden within several parts of Sokoto State. These findings highlight the importance of integrating environmental suitability, accessibility analysis, and surveillance data to identify operational silence zones and hidden severe malaria transmission landscapes.

3.2.4 Priority Index, Operational Silence Zones, and Healthcare Service Coverage

The integrated priority index (PI) revealed substantial spatial variation in malaria intervention priority across Sokoto State (Figure 11a). Priority scores ranged from 0.38 to 0.87, reflecting the combined influence of climate suitability, malaria endemicity, population exposure, and healthcare accessibility constraints. Four LGAs were classified as very high priority zones, including Kebbe (PI = 0.875), Tureta (0.708), Tambuwal (0.664), and Dange-Shuni (0.668), whereas Bodinga, Isa, Rabah, and Shagari were classified as high priority zones. Conversely, Gudu, Sabon Birni, Silame, Sokoto North, and Sokoto South were categorized as very low priority zones.

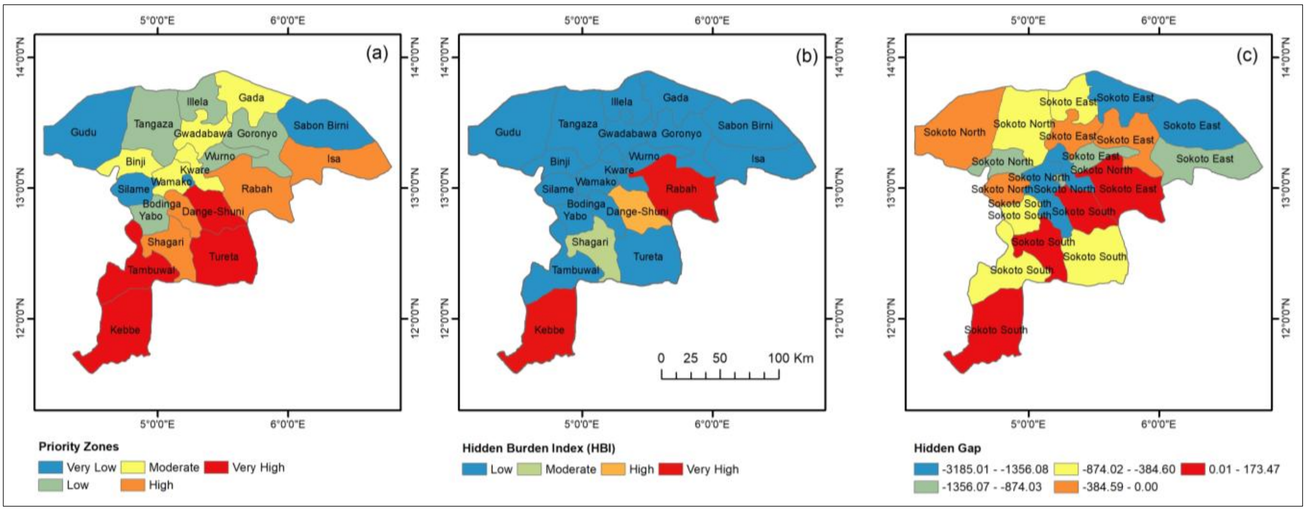

Figure 11. Spatial distribution of priority intervention zones, operational silence classes on the basis of the Hidden Burden Ratio (HBR), and hidden surveillance gaps across LGAs and wards in Sokoto State, Nigeria. Panel (a) shows malaria intervention priority zones derived from the integrated Priority Index; panel (b) illustrates operational silence classes indicating probable surveillance underdetection; and panel (c) presents the spatial distribution of hidden surveillance gaps, highlighting areas where the estimated climate-driven severe malaria burden exceeds reported surveillance records. These maps identify critical locations for targeted surveillance strengthening, healthcare accessibility improvement, and malaria control interventions.

Operational silence analysis further highlighted substantial disparities in surveillance performance across the state (Figure 11b). Rabah presented the highest Hidden Burden Ratio (11.04), followed by Kebbe (7.31), Dange-Shuni (3.03), and Shagari (1.95), indicating the probable underdetection of severe malaria burdens despite favorable environmental conditions for transmission. Consequently, Rabah and Kebbe were classified as very high operational silence zones, Dange-Shuni as high, and Shagari as moderate. Most remaining LGAs were classified as low-operational-valence LGAs, suggesting relatively better agreement between the estimated and reported malaria burdens.

Healthcare service coverage also demonstrated marked spatial variability. The number of health facilities ranged from only 21 facilities in Sokoto North to 73 facilities in Wamako. The population served per health facility varied substantially, ranging from 2,216 persons per facility in Silame to over 14,156 persons per facility in Sokoto North. High population-to-facility ratios were additionally observed in Dange-Shuni (11,342 persons per facility), Sokoto South (9,861), and Wamako (9,433), indicating potential pressure on healthcare resources and reduced surveillance efficiency.

The hidden-gap analysis revealed notable discrepancies between the estimated climate-driven severe malaria burden and reported surveillance records (Figure 11c). Positive hidden-gap values were observed in Rabah (+101.43 cases), Kebbe (+120.93 cases), Dange-Shuni (+173.47 cases), and Shagari (+67.57 cases), suggesting probable underreporting and concealed malaria transmission. In contrast, strongly negative hidden-gap values were observed in Gada (−3185.01 cases), Wamako (−3087.08 cases), Sabon Birni (−1826.32 cases), and Bodinga (−1407.76 cases), indicating comparatively stronger surveillance capture relative to the model-estimated burden.

Overall, the combined Priority Index, operational silence classification, healthcare service coverage indicators, and hidden-gap assessment (Figure 11) identified **Kebbe, Rabah, Dange-Shuni, Tureta, Tambuwal, and Shagari** as the most critical locations for strengthening malaria surveillance, improving healthcare accessibility, and implementing targeted intervention strategies in Sokoto State.

4. Discussion

The present study investigated the temporal dynamics, spatial heterogeneity, and climate-driven hidden severe malaria burden across Sokoto State, Nigeria, via an integrated geospatial epidemiological framework. The findings revealed strong temporal seasonality, substantial spatial variability among LGAs and wards, and pronounced operational surveillance gaps associated with poor healthcare accessibility and environmentally favorable transmission conditions.

The temporal analysis revealed substantial interannual variability in severe malaria burdens between 2014 and 2024, with particularly elevated burdens from 2014–2016 followed by relatively lower reported cases after 2018. Although the overall state-level Mann–Kendall trend was statistically nonsignificant, several LGAs exhibited strong localized increasing trends. These findings indicate that malaria transmission dynamics within Sokoto State are spatially heterogeneous rather than uniformly distributed across the state. Similar patterns of localized malaria persistence despite broader regional declines have been reported across several semiarid African environments where environmental suitability and healthcare accessibility vary considerably at local scales [42–44].

The pronounced seasonality observed in the present study is consistent with the hydroclimatic controls governing malaria transmission within the Sudan savannah ecological zone. Peak transmission occurs during and immediately after the rainy season when rainfall, soil moisture, humidity, and temporary surface water availability create favorable breeding habitats for Anopheles mosquitoes. Previous studies across West Africa have similarly demonstrated strong associations between rainfall seasonality and malaria transmission intensity [45–47]. Rainfall variability influences larval habitat formation, whereas temperature regulates mosquito survival and parasite development rates [48]. The strong seasonal concentration identified in the present study therefore supports the widely recognized climatic sensitivity of malaria transmission within semiarid tropical environments.

Climate suitability modeling further demonstrated that Sokoto State maintains highly favorable environmental conditions for sustained malaria transmission despite its semiarid setting. Temperature suitability remained consistently high across most LGAs, whereas rainfall and atmospheric moisture conditions strongly influenced spatial variability in transmission potential. These findings are consistent with mechanistic malaria-climate studies indicating that optimal malaria transmission commonly occurs under warm thermal conditions combined with seasonal moisture availability [49–51]. The integrated climate suitability index additionally demonstrated that the transmission potential within Sokoto State is governed by the combined effects of multiple environmental variables rather than by rainfall or temperature independently.

A major contribution of the present study is the identification of probable hidden severe malaria burdens and operational surveillance gaps via accessibility-constrained burden estimation. Several LGAs, particularly Rabah, Kebbe, and Dange-Shuni, presented substantially elevated Hidden Burden Ratios despite relatively lower reported surveillance records. These findings strongly suggest that reported severe malaria cases may substantially underestimate the actual transmission burden within poorly accessible and operationally underserved regions.

Previous studies have shown that healthcare accessibility strongly influences malaria detection, reporting efficiency, and treatment-seeking behavior [52–53]. Populations residing in geographically isolated settlements commonly experience delayed diagnosis, lower healthcare utilization, and reduced surveillance coverage, thereby increasing the likelihood of hidden transmission and underreporting [54]. The present findings support these observations and further demonstrate that accessibility limitations may create apparent low-burden conditions despite environmentally favorable transmission landscapes.

The ward-level hotspot analysis additionally revealed substantial microspatial heterogeneity in hidden transmission potential. Several wards within Tambuwal, Kebbe, and neighboring LGAs exhibited extremely high-priority classifications associated with elevated travel time, high climate suitability, and increased malaria endemicity. These findings emphasize the importance of fine-scale geospatial analysis for malaria surveillance and intervention planning. Aggregated state-level or LGA-level analyses may conceal highly localized transmission hotspots and operational silence zones within remote settlements.

The integrated priority index framework developed in this study further demonstrated the value of combining climate suitability, malaria endemicity, population exposure, and accessibility indicators for identifying hidden transmission landscapes. Previous malaria mapping studies have commonly focused on either environmental suitability or reported surveillance data independently [55–57]. In contrast, the present framework integrates both environmental and operational determinants of transmission, thereby providing a more comprehensive representation of severe malaria risk and surveillance vulnerability.

The findings also highlight important implications for malaria control policies and surveillance strengthening within northern Nigeria. LGAs identified as high operational silence zones may require the following:

- improved healthcare accessibility,
- enhanced surveillance coverage,
- targeted active case detection,
- accessibility-focused intervention planning, and
- strengthened healthcare infrastructure.

Remote and underserved settlements may particularly benefit from mobile health services, improved transportation connectivity, and localized surveillance strengthening programs.

Despite the robustness of the integrated framework, several limitations should be acknowledged. First, the study relied partly on reported severe malaria surveillance data, which may contain reporting inconsistencies and operational biases. Second, the climate-driven burden estimation framework represents the modeled transmission potential rather than the direct clinical incidence. Third, the use of static PfPR and population datasets may not fully capture short-term demographic and epidemiological variability during the study period. Additionally, healthcare accessibility was represented primarily through travel-time constraints and may not fully account for healthcare quality, affordability, or behavioral determinants influencing treatment-seeking patterns.

Future studies should integrate higher temporal resolution climate datasets, dynamic population mobility patterns, vector distribution data, and health facility utilization information to further refine hidden burden estimation. The incorporation of machine learning approaches, real-time climate forecasting, and mobile health surveillance systems may additionally improve operational malaria intelligence and early warning capabilities within semiarid African environments.

Overall, the present study demonstrated that severe malaria burden in Sokoto State is governed by the combined effects of environmental suitability, malaria endemicity, population exposure, and healthcare accessibility constraints. The integrated geospatial framework revealed substantial hidden transmission potential and operational surveillance gaps within several LGAs and wards, highlighting the importance of accessibility-sensitive malaria surveillance and targeted intervention planning within semiarid regions of sub-Saharan Africa.

Data availability statement: The data used in this study are open to access as follows:

The datasets used in this study were obtained from publicly available sources and institutional databases. Severe malaria surveillance records (2014–2024) were obtained from the Nigerian District Health Information System 2 (DHIS2) platform. Administrative boundary data were acquired from the Humanitarian Data Exchange (HDX), while health facility location data were obtained from GRID3 Nigeria. The population distribution data were sourced from WorldPop, the climate variables were derived from the ERA5-Land reanalysis dataset, and *Plasmodium falciparum* parasite rate (PfPR) data were obtained from the Malaria Atlas Project (MAP). Healthcare accessibility and travel-time datasets were generated by the authors through geospatial accessibility modeling. The datasets are available from the following sources: DHIS2 Nigeria, Humanitarian Data Exchange (HDX), GRID3 Data Hub, WorldPop, ERA5-Land, and Malaria Atlas Project. The processed datasets and analytical outputs generated during this study are available from the corresponding author upon reasonable request.

Author Contributions: Author Contributions: Conceptualization, Y.J.C. and Z.I.; methodology, Y.J.C., Z.I., and C.A.U.; software, Z.I.; validation, Z.I., Y.J.C., E.N.S., and U.M.I.; formal analysis, Z.I.; investigation, Y.J.C., C.A.U., E.N.S., A.M., M.M., U.M.I., and Y.J.D.; data curation, Y.J.C., U.M.I., and M.M.; visualization, Z.I.; writing—original draft preparation, Z.I. and Y.J.C.; writing—review and editing, C.A.U., E.N.S., A.M., M.M., U.M.I., and Y.J.D.; supervision, Y.J.C.; project administration, Y.J.C.; resources, C.A.U., E.N.S., A.M., M.M., U.M.I., and Y.J.D. All authors have read and agreed to the published version of the manuscript. All the authors have read and agreed to the published version of the manuscript.

Funding

This research received no external funding.

Informed Consent Statement

Not applicable.

Conflicts of interest

The authors declare that they have no conflicts of interest.

Abbreviations

The following abbreviations are used in this manuscript:

Abbreviation	
AC	Accessibility Constraint
ANOVA	Analysis of Variance
CSI	Climate Suitability Index
DHIS2	District Health Information System 2
ESM	Estimated Severe Malaria Burden
HBI	Hidden Burden Index
HBR	Hidden Burden Ratio
LGA	Local Government Area
PfPR	Plasmodium falciparum Parasite Rate
PI	Priority Index

References

1. World Health Organization (WHO). *World Malaria Report 2024*; WHO: Geneva, Switzerland, 2024.
2. Snow, R.W.; Sartorius, B.; Kyalo, D.; Maina, J.; Amratia, P.; Mundia, C.W.; Bejon, P.; Noor, A.M. The Prevalence of Plasmodium Falciparum in Sub-Saharan Africa Since 1900. *Nature* **2017**, *550*, 515–518, doi:10.1038/nature24059.
3. White, N.J.; Turner, G.D.H.; Medana, I.M.; Dondorp, A.M.; Day, N.P.J. The Murine Cerebral Malaria Phenomenon. *Trends in Parasitology* **2010**, *26*, 11–15, doi:10.1016/j.pt.2009.10.007.
4. Dondorp, A.M.; Fanello, C.I.; Hendriksen, I.C.; Gomes, E.; Seni, A.; Chhaganlal, K. D; Bojang, K.; Olaosebikan, R.; Anunobi, N.; Maitland, K.; et al. Artesunate versus Quinine in the Treatment of Severe Falciparum Malaria in African Children (AQUAMAT): An Open-Label, Randomized Trial. *The Lancet* **2010**, *376*, 1647–1657, doi:10.1016/s0140-6736(10)61924-1.
5. World Health Organization (WHO). *World Malaria Report 2023*; WHO: Geneva, Switzerland, 2023.
6. National Malaria Elimination Programme (NMEP); National Population Commission (NPopC); National Bureau of Statistics (NBS); ICF International. *Nigeria Malaria Indicator Survey 2021*; Abuja, Nigeria, 2022.
7. Aregawi, M.W.; Ali, A.S.; Al-mafazy, A.; Molteni, F.; Katikiti, S.; Warsame, M.; Njau, R.J.; Komatsu, R.; Korenromp, E.; Hosseini, M.; et al. Reductions in Malaria and Anemia Case and Death Burden at Hospitals Following Scale-Up of Malaria Control in Zanzibar, 1999-2008. *Malaria Journal* **2011**, *10*, doi:10.1186/1475-2875-10-46.
8. Mordecai, E.A.; Cohen, J.M.; Evans, M.V.; Gudapati, P.; Johnson, L.R.; Lippi, C.A.; Miazgowicz, K.; Murdock, C.C.; Rohr, J.R.; Ryan, S.J.; et al. Detecting the Impact of Temperature on Transmission of Zika, Dengue, and Chikungunya Using Mechanistic Models. *PLOS Neglected Tropical Diseases* **2017**, *11*, e0005568, doi:10.1371/journal.pntd.0005568.
9. Caminade, C.; Kovats, S.; Rocklov, J.; Tompkins, A.M.; Morse, A.P.; Colón-González, F.J.; Stenlund, H.; Martens, P.; Lloyd, S.J. Impact of Climate Change on Global Malaria Distribution. *Proceedings of the National Academy of Sciences* **2014**, *111*, 3286–3291, doi:10.1073/pnas.1302089111.
10. Siraj, A.S.; Santos-Vega, M.; Bouma, M.J.; Yadeta, D.; Carrascal, D.R.; Pascual, M. Altitudinal Changes in Malaria Incidence in Highlands of Ethiopia and Colombia. *Science* **2014**, *343*, 1154–1158, doi:10.1126/science.1244325.
11. Beck-Johnson, L.M.; Nelson, W.A.; Paaijmans, K.P.; Read, A.F.; Thomas, M.B.; Bjørnstad, O.N. The Effect of Temperature on Anopheles Mosquito Population Dynamics and the Potential for Malaria Transmission. *PLoS ONE* **2013**, *8*, e79276, doi:10.1371/journal.pone.0079276.
12. Parham, P.E.; Michael, E. Modeling the Effects of Weather and Climate Change on Malaria Transmission. *Environmental Health Perspectives* **2010**, *118*, 620–626, doi:10.1289/ehp.0901256.
13. Thomson, M.C.; Connor, S.J.; Milligan, P.; Flasse, S.P. Mapping Malaria Risk in Africa: What Can Satellite Data Contribute? *Parasitology Today* **1997**, *13*, 313–318, doi:10.1016/s0169-4758(97)01097-1.
14. JA; Climate Change and Vector-Borne Diseases: A Regional Analysis. *Bulletin of the World Health Organization* **2026**, *78*.
15. Tanser, F.C.; Sharp, B.; le Sueur, D. Potential Effect of Climate Change on Malaria Transmission in Africa. *The Lancet* **2003**, *362*, 1792–1798, doi:10.1016/s0140-6736(03)14898-2.
16. Ermert, V.; Fink, A.H.; Jones, A.E.; Morse, A.P. Development of a New Version of the Liverpool Malaria Model. I. Refining the Parameter Settings and Mathematical Formulation of Basic Processes Based on a Literature Review. *Malaria Journal* **2011**, *10*, doi:10.1186/1475-2875-10-35.
17. Noor, A.M.; Zurovac, D.; Hay, S.I.; Ochola, S.A.; Snow, R.W. Defining equity in physical access to clinical services using geographical information systems. *Trop. Med. Int. Health* **2003**, *8*, 917–926.
18. Weiss, D.J.; Dzianach, P.A.; Saddler, A.; Lubinda, J.; Browne, A.; McPhail, M.; Rumisha, S.F.; Sanna, F.; Gelaw, Y.; Kiss, J.B.; et al. Mapping the Global Prevalence, Incidence, and Mortality of Plasmodium Falciparum and Plasmodium Vivax Malaria, 2000–22: A Spatial and Temporal Modeling Study. *The Lancet* **2025**, *405*, 979–990, doi:10.1016/s0140-6736(25)00038-8.
19. Tatem, A.J.; Smith, D.L. International Population Movements and Regional *Plasmodium Falciparum* Malaria Elimination Strategies. *Proceedings of the National Academy of Sciences* **2010**, *107*, 12222–12227, doi:10.1073/pnas.1002971107.
20. Bhatt, S.; Weiss, D.J.; Cameron, E.; Bisanzio, D.; Mappin, B.; Dalrymple, U.; Battle, K.E.; Moyes, C.L.; Henry, A.; Eckhoff, P.A.; et al. The effect of malaria control on *Plasmodium falciparum* in Africa between 2000 and 2015. *Nature* **2015**, *526*, 207–211.

21. Noor, A.M.; Amin, A.A.; Gething, P.W.; Atkinson, P.M.; Hay, S.I.; Snow, R.W. Modeling Distances Traveled to Government Health Services in Kenya. *Tropical Medicine & International Health* **2006**, *11*, 188–196, doi:10.1111/j.1365-3156.2005.01555.x.
22. Alegana, V.A.; Wright, J.A.; Pentrina, U.; Noor, A.M.; Snow, R.W.; Atkinson, P.M. Spatial Modeling of Healthcare Utilization for Treatment of Fever in Namibia. *International Journal of Health Geographics* **2012**, *11*, 6, doi:10.1186/1476-072x-11-6.
23. Tusting, L.S.; Bottomley, C.; Gibson, H.; Kleinschmidt, I.; Tatem, A.J.; Lindsay, S.W.; Gething, P.W. Housing Improvements and Malaria Risk in Sub-Saharan Africa: A Multi-Country Analysis of Survey Data. *PLOS Medicine* **2017**, *14*, e1002234, doi:10.1371/journal.pmed.1002234.
24. Stresman, G.H. Beyond Temperature and Precipitation: Ecological Risk Factors That Modify Malaria Transmission. *Acta Tropica* **2010**, *116*, 167–172, doi:10.1016/j.actatropica.2010.08.005.
25. Bousema, T.; Okell, L.; Felger, I.; Drakeley, C. Asymptomatic Malaria Infections: Detectability, Transmissibility and Public Health Relevance. *Nature Reviews Microbiology* **2014**, *12*, 833–840, doi:10.1038/nrmicro3364.
26. Wesolowski, A.; Eagle, N.; Tatem, A.J.; Smith, D.L.; Noor, A.M.; Snow, R.W.; Buckee, C.O. Quantifying the Impact of Human Mobility on Malaria. *Science* **2012**, *338*, 267–270, doi:10.1126/science.1223467.
27. Onyiri, N. Estimating Malaria Burden in Nigeria: A Geostatistical Modeling Approach. *Geospatial Health* **2015**, *10*, doi:10.4081/gh.2015.306.
28. Ryan, S.J.; Carlson, C.J.; Mordecai, E.A.; Johnson, L.R. Global Expansion and Redistribution of Aedes-Borne Virus Transmission Risk with Climate Change. *PLOS Neglected Tropical Diseases* **2019**, *13*, e0007213, doi:10.1371/journal.pntd.0007213.
29. Paaijmans, K.P.; Read, A.F.; Thomas, M.B. Understanding the Link between Malaria Risk and Climate. *Proceedings of the National Academy of Sciences* **2009**, *106*, 13844–13849, doi:10.1073/pnas.0903423106.
30. Hay, S.I.; Guerra, C.A.; Tatem, A.J.; Noor, A.M.; Snow, R.W. The Global Distribution and Population at Risk of Malaria: Past, Present, and Future. *The Lancet Infectious Diseases* **2004**, *4*, 327–336, doi:10.1016/s1473-3099(04)01043-6.
31. Tatem, A.J.; Gething, P.W.; Smith, D.L.; Hay, S.I. Urbanization and the global malaria recession. *Malar. J.* **2013**, *12*, 133.
32. Guerra, C.A.; Noor, A.M.; Myint, H.Y.; Hay, S.I. The limits and intensity of *Plasmodium falciparum* transmission: Implications for malaria control and elimination worldwide. *PLoS Med.* **2008**, *5*, e38.
33. Federal Ministry of Health. (2025). *District Health Information System 2 (DHIS2) Nigeria*. Federal Ministry of Health, Nigeria. https://dhis2nigeria.org.ng
34. United Nations Office for the Coordination of Humanitarian Affairs. (2025). *Humanitarian Data Exchange (HDX): Nigeria administrative boundaries*. OCHA. https://data.humdata.org
35. GRID3. (2025). *Nigeria health facility database*. Geo-Referenced Infrastructure and Demographic Data for Development (GRID3). https://data.grid3.org
36. WorldPop. (2025). *WorldPop population distribution datasets*. School of Geography and Environmental Science, University of Southampton. https://www.worldpop.org
37. Muñoz Sabater, J. (2019). *ERA5-Land hourly data from 1950 to present*. Copernicus Climate Change Service (C3S) Climate Data Store (CDS). https://www.ecmwf.int/en/era5-land
38. Weiss, D. J., Lucas, T. C. D., Nguyen, M., Nandi, A. K., Bisanzio, D., Battle, K. E., Cameron, E., Twohig, K. A., Pfeffer, D. A., Rozier, J. A., Gibson, H. S., Rao, P. C., Casey, D., Bertozzi-Villa, A., Collins, E. L., Dalrymple, U., Gray, N., Harris, J. R., Howes, R. E., ... Gething, P. W. (2019). Mapping the global prevalence, incidence, and mortality of *Plasmodium falciparum*, 2000–2017: A spatial and temporal modeling study. *The Lancet, 394*(10195), 322–331. https://doi.org/10.1016/S0140-6736(19)31097-9
39. Malaria Atlas Project. (2025). *Plasmodium falciparum parasite rate (PfPR) raster datasets*. Malaria Atlas Project. https://malariaatlas.org
40. Mann, H. B. (1945). Nonparametric tests against trend. *Econometrica, 13*(3), 245–259. https://doi.org/10.2307/1907187
41. Sen, P. K. (1968). Estimates of the regression coefficient based on Kendall's tau. *Journal of the American Statistical Association, 63*(324), 1379–1389. https://doi.org/10.1080/01621459.1968.10480934
42. World Health Organization (WHO). World Malaria Report 2024; WHO: Geneva, Switzerland, 2024.
43. World Health Organization (WHO). World Malaria Report 2023; WHO: Geneva, Switzerland, 2023.

44. Bhatt, S.; Weiss, D.J.; Cameron, E.; Bisanzio, D.; Mappin, B.; Dalrymple, U.; Battle, K.E.; Moyes, C.L.; Henry, A.; Eckhoff, P.A.; et al. The Effect of Malaria Control on Plasmodium Falciparum in Africa between 2000 And 2015. *Nature* **2015**, *526*, 207–211, doi:10.1038/nature15535.
45. JA; Climate Change and Vector-Borne Diseases: A Regional Analysis. *Bulletin of the World Health Organization* **2026**, *78*.
46. Tanser, F.C.; Sharp, B.; le Sueur, D. Potential Effect of Climate Change on Malaria Transmission in Africa. *The Lancet* **2003**, *362*, 1792–1798, doi:10.1016/s0140-6736(03)14898-2.
47. Ermert, V.; Fink, A.H.; Jones, A.E.; Morse, A.P. Development of a New Version of the Liverpool Malaria Model. I. Refining the Parameter Settings and Mathematical Formulation of Basic Processes Based on a Literature Review. *Malaria Journal* **2011**, *10*, doi:10.1186/1475-2875-10-35.
48. Paaijmans, K.P.; Read, A.F.; Thomas, M.B. Understanding the Link between Malaria Risk and Climate. *Proceedings of the National Academy of Sciences* **2009**, *106*, 13844–13849, doi:10.1073/pnas.0903423106.
49. Mordecai, E.A.; Cohen, J.M.; Evans, M.V.; Gudapati, P.; Johnson, L.R.; Lippi, C.A.; Miazgowicz, K.; Murdock, C.C.; Rohr, J.R.; Ryan, S.J.; et al. Detecting the Impact of Temperature on Transmission of Zika, Dengue, and Chikungunya Using Mechanistic Models. *PLOS Neglected Tropical Diseases* **2017**, *11*, e0005568, doi:10.1371/journal.pntd.0005568.
50. Caminade, C.; Kovats, S.; Rocklov, J.; Tompkins, A.M.; Morse, A.P.; Colón-González, F.J.; Stenlund, H.; Martens, P.; Lloyd, S.J. Impact of climate change on global malaria distribution. Proc. Natl. Acad. Sci. USA 2014, 111, 3286–3291. https://doi.org/10.1073/pnas.1302089111.
51. Beck-Johnson, L.M.; Nelson, W.A.; Paaijmans, K.P.; Read, A.F.; Thomas, M.B.; Bjørnstad, O.N. The Effect of Temperature on Anopheles Mosquito Population Dynamics and the Potential for Malaria Transmission. *PLoS ONE* **2013**, *8*, e79276, doi:10.1371/journal.pone.0079276.
52. Alegana, V.A.; Wright, J.A.; Pentrina, U.; Noor, A.M.; Snow, R.W.; Atkinson, P.M. Spatial modeling of healthcare utilization for treatment of fever in Namibia. Int. J. Health Geogr. 2012, 11, 6. https://doi.org/10.1186/1476-072X-11-6.
53. Noor, A.M.; Zurovac, D.; Hay, S.I.; Ochola, S.A.; Snow, R.W. Defining equity in physical access to clinical services using geographical information systems. Trop. Med. Int. Health 2003, 8, 917–926. https://doi.org/10.1046/j.1365-3156.2003.01100.x.
54. Wesolowski, A.; Eagle, N.; Tatem, A.J.; Smith, D.L.; Noor, A.M.; Snow, R.W.; Buckee, C.O. Quantifying the impact of human mobility on malaria. Science 2012, 338, 267–270. https://doi.org/10.1126/science.1223467.
55. Weiss, D.J.; Lucas, T.C.D.; Nguyen, M.; Nandi, A.K.; Bisanzio, D.; Battle, K.E.; Cameron, E.; Twohig, K.A.; Pfeffer, D.A.; Rozier, J.A.; et al. Mapping the global prevalence, incidence, and mortality of Plasmodium falciparum, 2000–2017. Lancet 2019, 394, 322–331. https://doi.org/10.1016/S0140-6736(19)31097-9.
56. Tatem, A.J.; Smith, D.L. International population movements and regional Plasmodium falciparum malaria elimination strategies. Proc. Natl. Acad. Sci. USA 2010, 107, 12222–12227. https://doi.org/10.1073/pnas.1002971107.
57. Guerra, C.A.; Noor, A.M.; Myint, H.Y.; Hay, S.I. The limits and intensity of Plasmodium falciparum transmission: Implications for malaria control and elimination worldwide. PLoS Med. 2008, 5, e38. https://doi.org/10.1371/journal.pmed.0050038.